Magnetic properties and hyperfine interactions in Cr8, Cr7Cd, and Cr7Ni molecular rings from 19F-NMR

L. Bordonali, E. Garlatti, C. M. Casadei, Y. Furukawa, A. Lascialfari, S. Carretta, F. Troiani, G. Timco, R. E. P. Winpenny, and F. Borsa

Citation: The Journal of Chemical Physics **140**, 144306 (2014); doi: 10.1063/1.4870469
View online: http://dx.doi.org/10.1063/1.4870469
View Table of Contents: http://scitation.aip.org/content/aip/journal/jcp/140/14?ver=pdfcov
Published by the AIP Publishing

Magnetic properties and hyperfine interactions in Cr_8, Cr_7Cd, and Cr_7Ni molecular rings from ^{19}F-NMR

L. Bordonali,[1,2,3] E. Garlatti,[4,5] C. M. Casadei,[1,3] Y. Furukawa,[3] A. Lascialfari,[1,2,4] S. Carretta,[5] F. Troiani,[6] G. Timco,[7] R. E. P. Winpenny,[7] and F. Borsa[1,2,3]
[1]*Department of Physics, Università di Pavia, I-27100 Pavia, Italy*
[2]*Consorzio INSTM, Via Giusti 9, I-50121 Firenze, Italy*
[3]*Department of Physics and Astronomy, Ames Laboratory, Iowa State University, Ames, Iowa 50011, USA*
[4]*Department of Physics, Università degli Studi di Milano, Via Celoria 16, 20133 Milano, Italy*
[5]*Dipartimento di Fisica e Scienze della Terra, Università di Parma, Viale G. P. Usberti 7/A, 43124 Parma, Italy*
[6]*S3 Istituto Nanoscienze, Consiglio Nazionale delle Ricerche, I-4100 Modena, Italy*
[7]*The Lewis Magnetism Laboratory, The University of Manchester, M13 9PL Manchester, United Kingdom*

(Received 26 December 2013; accepted 14 March 2014; published online 11 April 2014)

A detailed experimental investigation of the ^{19}F nuclear magnetic resonance is made on single crystals of the homometallic Cr_8 antiferromagnetic molecular ring and heterometallic Cr_7Cd and Cr_7Ni rings in the low temperature ground state. Since the F^- ion is located midway between neighboring magnetic metal ions in the ring, the ^{19}F-NMR spectra yield information about the local electronic spin density and ^{19}F hyperfine interactions. In Cr_8, where the ground state is a singlet with total spin $S_T = 0$, the ^{19}F-NMR spectra at 1.7 K and low external magnetic field display a single narrow line, while when the magnetic field is increased towards the first level crossing field, satellite lines appear in the ^{19}F-NMR spectrum, indicating a progressive increase in the Boltzmann population of the first excited state $S_T = 1$. In the heterometallic rings, Cr_7Cd and Cr_7Ni, whose ground state is magnetic with $S_T = 3/2$ and $S_T = 1/2$, respectively, the ^{19}F-NMR spectrum has a complicated structure which depends on the strength and orientation of the magnetic field, due to both isotropic and anisotropic transferred hyperfine interactions and classical dipolar interactions. From the ^{19}F-NMR spectra in single crystals we estimated the transferred hyperfine constants for both the F^--Ni^{2+} and the F^--Cd^{2+} bonds. The values of the hyperfine constants compare well to the ones known for F^--Ni^{2+} in $KNiF_3$ and NiF_2 and for F^--Cr^{3+} in K_2NaCrF_6. The results are discussed in terms of hybridization of the 2s, 2p orbitals of the F^- ion and the d orbitals of the magnetic ion. Finally, we discuss the implications of our results for the electron-spin decoherence. © *2014 AIP Publishing LLC*. [http://dx.doi.org/10.1063/1.4870469]

I. INTRODUCTION

Molecular magnets have received much attention ever since their potential use in the field of quantum information processing (QIP) had been recognized;[1,2] recently, a suitable physical support for QIP was found in antiferromagnetic (AFM) heterometallic wheels.[3,4] These rings are composed of a controllable number of transition metal ions arranged in the fashion of a planar ring. Each ion is coupled with its nearest-neighbors via a strong antiferromagnetic exchange interaction, J. Due to the negligible interaction among the magnetic moments across the ring, as compared to the nearest-neighbors coupling along the ring J, and to the negligible inter-molecular interaction as compared to J, AFM rings are considered excellent prototypes for the theoretical and experimental investigation of zero dimensional magnets.[5] Specific examples are provided by the Cr_7Cd and Cr_7Ni antiferromagnetic rings, consisting of one Cd^{2+} (Ni^{2+}) ion and seven Cr^{3+} ions forming an octagonal ring. Contrary to its homonuclear parent, Cr_8, having total spin $S_T = 0$ in the ground state,[6] the total ground state spin of the Cr_7Cd molecule is $S_T = 3/2$, while in the Cr_7Ni molecule is $S_T = 1/2$,[7] since the presence of a diamagnetic ($s = 0$) and $s = 1$ ion, respectively, breaks the symmetric configuration of the AFM aligned Cr^{3+} ($s = 3/2$) spins.[8–13]

The experimental investigation of the magnetic properties and the spin dynamics in heterometallic AFM rings is particularly important for a complete understanding of the mechanisms affecting the quantum coherence and decoherence in these systems. In this respect, nuclear magnetic resonance (NMR) is an excellent choice for probing local magnetic properties, and it has already proved useful in understanding the static and dynamic properties of a significant number of molecular magnets.[14]

From the analysis of NMR data it is indeed possible to extract the strength of the hyperfine interactions within the molecules. Couplings between the magnetic centers and the nuclei of nearby atoms are considered the main source of decoherence of the spin dynamics in these systems. Spin coherence deterioration can be identified as the major obstacle for the implementation of molecular magnets as QIP devices, since control over such devices implies the possibility of manipulating the superposition of quantum state on a short timescale with respect to the relaxation time of the spin system.[15]

It has already been experimentally proved that in AFM wheels, and in particular in Cr_7Ni, dipolar couplings with

protons represent the main source of decoherence.[16,17] On one hand, we would expect, *a priori*, that the coupling to the ^{19}F nuclei would introduce a substantial contribution to the decoherence, given the magnitude of the transferred spin density from the Cr^{3+} to the fluorine site. On the other hand, claims about the low/non-existent coupling of Fluorine nuclei with the electron spin have not been backed by an estimate of the interaction strength.

In this work we present the first detailed experimental investigation of the ^{19}F-NMR in the homometallic Cr_8 antiferromagnetic molecular ring and in the heterometallic Cr_7Cd and Cr_7Ni rings at low temperature, and as a function of the strength and orientation of the magnetic field in single crystal samples.

Since the F^- ion is located midway between two magnetic metal ions in the ring, the ^{19}F-NMR spectra are an excellent probe of the local spin density of the magnetic ions. In Cr_8 we find that the dependence of the local magnetic moment on the external field is due to the reduction of the gap between the low-lying multiplets: when the gap between the singlet $S_T = 0$ ground state and the first $S_T = 1$ excited state is comparable to the thermal energy, i.e., near the ground state level crossing at $H = \sim 7.6$ T, the molecule ensemble will be composed of a Boltzmann distribution of molecules in the ground state and in the first excited state. Within this framework, we argue that our observations indicate that at 1.7 K the lifetime of the excited state is longer than the shutter time of the NMR experiment (i.e., a few microseconds). ^{19}F-NMR spectra of the heterometallic rings Cr_7Cd and Cr_7Ni, having a magnetic ground state, display a more complicated, field-dependent structure, due to both isotropic and anisotropic transferred hyperfine interactions and classical dipolar interactions. The spectra can be interpreted on the basis of the theoretically calculated local magnetic moment distribution along the ring, and taking into account both the long-range classical dipolar interactions and the ^{19}F transferred hyperfine interaction with the magnetic Cr^{3+} and Ni^{2+} ions.

The presented results serve as the starting point to model decoherence effect related to the presence of Cr_7Ni-^{19}F couplings, and understand the reasons underlying the seemingly small relevance of this decoherence path.

II. SAMPLES: STRUCTURE AND MAGNETIC PROPERTIES

A. Structural properties

$Cr_8F_8Piv_{16}$ [Piv^- = Pivalate, trimethylacetate: $(CH_3)_3CCOO^-$], Cr_8 in short, is a widely studied homometallic antiferromagnetic molecular ring. The molecule is composed by eight almost coplanar Cr^{3+} magnetic ions whose electronic configuration is: $[Cr^{3+}] = [Ar]\ 3d^3$, $s = 3/2$. Adjacent Cr^{3+} ions are connected by one F^- bridging ion and two Pivalate bridging ligands.

Heterometallic analogues of the homometallic neutral wheel Cr_8 have been prepared by replacing a single Cr^{3+} center by a dication M^{2+}. The monoanionic heterometallic species $[Cr_7MF_8Piv_{16}]^-$ is therefore formed, and in the presence of a suitable cation it is possible to separate the heterometallic species from the homometallic compound based on the principle that a cation-anion pair has different crystallization properties than a neutral species. Details about the synthesis and the structural properties can be found in Ref. 18. A picture of the molecular rings and site labeling scheme is shown in Fig. 1, where only the atoms relevant for the present work are shown.

B. Distribution of the local spin density along the ring at low temperature

To analyze the ^{19}F-NMR spectra and to extract information about the hyperfine interactions, we rely on the values of the local spin density in the ring calculated theoretically. This is justified by the fact that the previous comparison of the calculated spins density and the one determined directly by ^{53}Cr-NMR[19,20] and neutron scattering[21] experiments in the same rings lead to an excellent agreement.

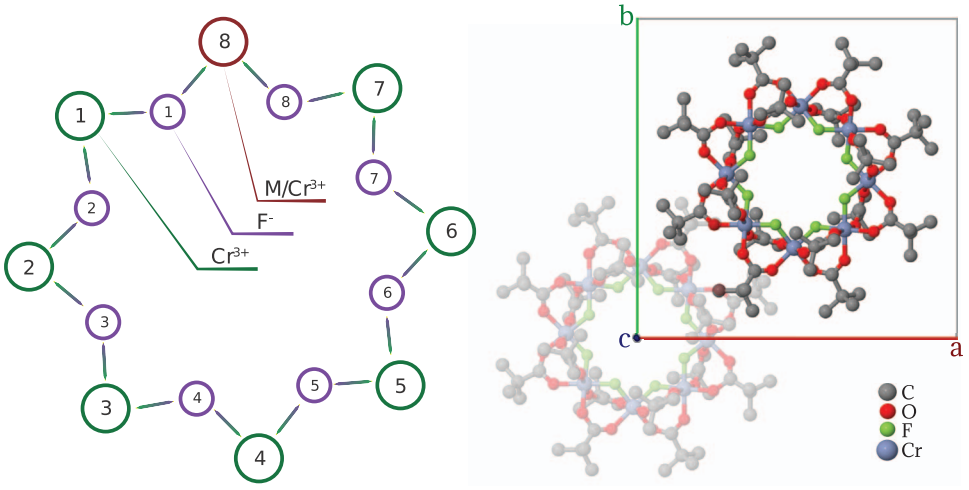

FIG. 1. (Left) Cr^{3+} and F^- ions labeling in use for the Cr_7M heterometallic rings: M = Cd^{2+}, Ni^{2+}. (Right) Cr_7M (M^{2+} = Cd^{2+}, Ni^{2+}) heterometallic ring unit cell viewed along the *c* axis, which is perpendicular to the ring's plane. Each molecular ring includes one ammonium ion at its center, not shown in this figure. The heterometallic site occupies a random position on the ring, and therefore has not been labeled. Hydrogen atoms are not shown for simplicity.

The low-temperature properties of Cr_7M AFM wheels can be described by the following spin Hamiltonian:

$$\mathcal{H} = \sum_{i=1}^{N} J_{i,i+1} \boldsymbol{s}_i \cdot \boldsymbol{s}_{i+1} + \sum_{i=1}^{N} d_i \left[s_{z,i}^2 - \frac{1}{3} s_i(s_i+1) \right] + \sum_{i>j=1}^{N} D_{i,j} [2 s_{z,i} s_{z,j} - s_{x,i} s_{x,j} - s_{y,i} s_{y,j}] + \mu_B \sum_{i=1}^{N} g_i \boldsymbol{H} \cdot \boldsymbol{s}_i, \quad (1)$$

where s_i is the spin operator of the ith magnetic ion ($s_i = 3/2$ for Cr^{3+} ions, $s_i = 0$ for the Cd^{2+} ion, and $s_i = 1$ for the Ni^{2+} ion). The first term represents the Heisenberg nearest-neighbors exchange interaction, with the usual cyclic boundary condition $N + 1 = 1$, N being the number of metal ions in the molecule (here $N = 8$). The second term accounts for uniaxial local crystal fields (being z the axis perpendicular to the plane of the ring). The third term in Eq. (1) is the axial contribution to the dipolar anisotropic intra-cluster spin-spin interaction, where $D_{i,j}$ is evaluated within the point-dipole approximation. The last term is the Zeeman coupling to an external field. The parameters of the above Hamiltonian were determined by means of inelastic neutron scattering (INS) and thermodynamic measurements.[13,22–24]

Note that the present convention for the expression of the magnetic moment is $\boldsymbol{\mu} = -g\langle \boldsymbol{s} \rangle \mu_B$, i.e., $\boldsymbol{\mu}$ is anti-parallel[39] to $\boldsymbol{s}$.

The eigenstates and eigenvalues of the Hamiltonian in Eq. (1) calculated with the procedure detailed in Refs. 22 and 13 have been exploited to evaluate the magnetic field dependence of the thermal averages (specified by the subscript "Th") of the local spin operators $s_{\alpha,i}$ ($\alpha = x, y, z$), $\langle s_{\alpha,i} \rangle_{\mathrm{Th}} = 1/Z \sum_{j=1}^{n} \langle j | s_{\alpha,i} | j \rangle e^{-\beta E_j(H)}$ where the index i labels the Cr^{3+} (and Ni^{2+}) sites and the sum runs over the eigenstates and eigenvalues, which depend on the applied field H. If the magnetic field is applied along the crystal c-axis, perpendicular to the ring's plane ($\theta = 0$ or $\boldsymbol{H} \parallel c$), only $\langle s_{z,i} \rangle_{\mathrm{Th}} \neq 0$ while if the magnetic field is applied parallel to the ring's plane ($\theta = \pi/2$ or $\boldsymbol{H} \perp c$) only $\langle s_{k,i} \rangle_{\mathrm{Th}} \neq 0$, where k denotes the orientation of magnetic field in any of the possible in-plane directions, which are all equivalent due to the cylindrical symmetry of the spin Hamiltonian in Eq. (1). In Secs. II C–II E we identify z with the c axis of the molecular wheel, which is perpendicular to the plane of the ring; i.e., $z \equiv c$.

C. Cr_8

The relevant result to be used here is that the ground state is practically a $S_T = 0$ singlet state and the first excited state is a crystal field split triplet $S_T = 1$ state.

In zero applied field the ground state is $|S, M_S\rangle = |0, 0\rangle$. As an external field is applied, the excited state $|1, -1\rangle$, initially at 9.2 K above the ground state, lowers progressively its energy, crossing the $|0, 0\rangle$ state at $H_c = 6.9$ T if $\boldsymbol{H} \perp c$.

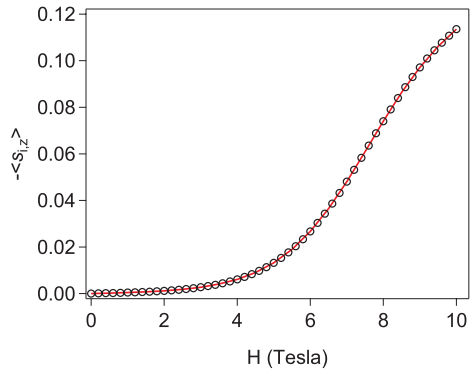

FIG. 2. Plot of the calculated expectation value of the local spin z-component as a function of the external field in Cr_8 at $T = 1.7$ K (circles), taking into account the contributions of all Cr_8 energy levels. The magnetic field is oriented perpendicular to the plane of the ring. The full line represents the expectation value of the local spin calculated by taking into account the thermal population of the first excited state only.

In the $S_T = 0$ ground state the macroscopic magnetization M as well as the local spin expectation value of the Cr^{3+} ions are zero. By increasing the magnetic field, the excited state becomes progressively populated and both the magnetization M and the local spin expectation value increase. This is shown in Fig. 2.

Note that the local spin expectation value in Fig. 2 is calculated by either including all the excited states (black circles in Fig. 2) or only the first excited state (full line in Fig. 2). The comparison of the two sets of data shows that at $T = 1.7$ K the magnetic properties are entirely determined, up to 10 T, by the thermal mixing of the $S_T = 0$ ground state and the $|1, -1\rangle$ branch of the first triplet excited state $S_T = 1$.

It should be stressed, however, that both calculations of the local spin represent thermal average values. Only a local probe like NMR can distinguish between these two possible scenarios: (a) when the phonon-induced dynamics of electronic spins are faster than nuclear ones, NMR local probes, such as F^- nuclei, see all the rings with a uniform local spin value given by the thermal averages reported in Fig. 2; (b) when the characteristic times of electronic spin dynamics are comparable with the nuclear ones, nuclei probe both the singlet ground state and the triplet excited state, where the total spin $S_T = 1$ is homogeneously distributed over the 8 equivalent Cr^{3+} sites, yielding $\langle s \rangle = S_T/8$.

D. Cr_7Cd

Upon substitution of one magnetic Cr^{3+} ion by means of a diamagnetic Cd^{2+} ion the symmetry in the ring is broken and the ground state becomes a magnetic $S_T = 3/2$ state. Also, the local spin density in the ground state is different from zero and is site dependent. Its distribution in the ring has been calculated, and the theoretical results were shown to be in excellent agreement with the ^{53}Cr-NMR results.[19] The values of the non-uniform local spin densities for two orientations of the external magnetic field are reported in Table I.

TABLE I. Expectation values of the local spin $\langle s \rangle$ at $T = 1.7$ K, $H = 6$ T, in the first excited state for Cr_8 and in the ground state for Cr_7Cd[19] and Cr_7Ni.[20] Values are shown for two orientations of the ring, i.e., $\theta = 0, \pi/2$.

	Cr_8		Cr_7Cd		Cr_7Ni	
Site	$\theta = 0$	$\theta = \pi/2$	$\theta = 0$	$\theta = \pi/2$	$\theta = 0$	$\theta = \pi/2$
Cr-1	−0.125	−0.124	−1.077	−1.010	−0.657	−0.461
Cr-2	−0.126	−0.124	0.849	0.750	0.563	0.352
Cr-3	−0.125	−0.124	−0.959	−0.870	−0.625	−0.432
Cr-4	−0.125	−0.124	0.875	0.760	0.563	0.349
Cr-5	−0.124	−0.124	−0.959	−0.870	−0.625	−0.432
Cr-6	−0.125	−0.124	0.849	0.750	0.563	0.352
Cr-7	−0.124	−0.124	−1.077	−1.010	−0.657	−0.461
Cr-8/Cd/Ni	−0.125	−0.124	0	0	0.375	0.230

E. Cr_7Ni

Upon substitution of one $s = 3/2$ Cr^{3+} ion with the $s = 1$ Ni^{2+} ion the ring's magnetic ground state becomes a total spin $S_T = 1/2$ state. The first excited state is a total spin $S_T = 3/2$ state split by anisotropy effects at more than 10 K above the ground state, which does not affect the low temperature data presented in this paper, since all NMR measurements have been carried out at external fields far from the ground state level crossing. The site dependent local spin density redistribution in the ring was calculated theoretically and the values were found in good agreement with ^{53}Cr-NMR results.[20] The values of the local spin densities for two orientations of the external magnetic field are shown in Table I.

It should be stressed here that the significant anisotropy of the local magnetic moments of Cr_7Ni in its otherwise isotropic $S_T = 1/2$ ground state is due to the presence of S-mixing with the excited anisotropic $S_T = 3/2$ states.[40]

III. ^{19}F-NMR EXPERIMENTAL RESULTS

The ^{19}F-NMR experiments were performed on a pulse Fourier Transform (FT) spectrometer and a 9 T variable field superconducting magnet. Most of the measurements were performed in a liquid helium bath cryostat at 1.7 K. The detected signal is the solid-spin-echo signal following the Hahn sequence of pulses $\pi/2$-τ-$\pi/2$-τ-echo.

Since most spectra are broad and structured, the whole NMR line could not be irradiated by means of a single radio frequency (RF) pulse and thus a field-sweep method was adopted to collect the ^{19}F spectra. The radio frequency is kept fixed while the applied magnetic field is swept over a selected range around the resonance Larmor field of the bare nucleus. Pulse sequences are repeated continuously during the sweep with a delay time named repetition time $t_{Rep} \sim 100$ ms. The spectrum y-value is given, at any field value, by the integral of the acquired spin-echo signal following the Hahn sequence. Every spectral point is then calculated as the running average over the last N_{Avg} acquisitions.

In order to resolve the fine structure in the spectrum it is required that the magnetic field variation during one point acquisition is small compared to the width of the spectral structures of interest. The use of a fast repetition rate, i.e., t_{Rep} ~100 ms is necessary to improve the signal-to-noise ratio.

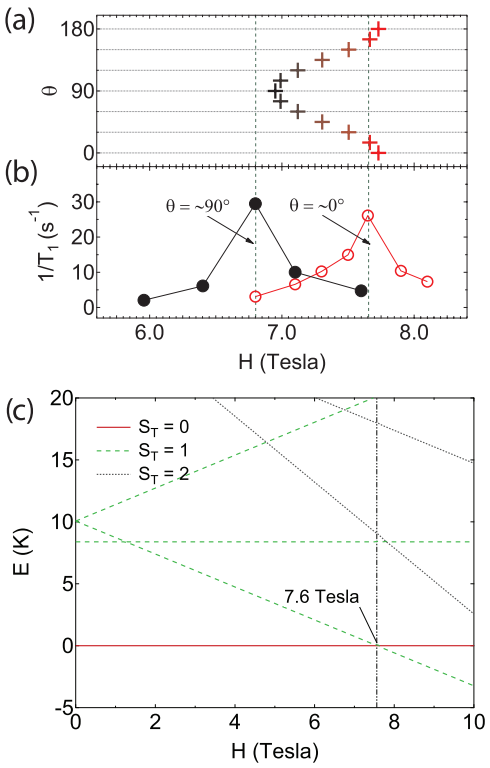

FIG. 3. (a) Theoretical dependence of the first ground state level crossing field H_c in Cr_8 on the polar angle θ. The axes are swapped to better illustrate the comparison with the experiment; (b) field dependence of the ^{1}H-NMR nuclear spin-lattice relaxation rates for two different orientation of the Cr_8 crystal with respect to the external field H; (c) ground state and first excited magnetic energy levels in Cr_8, with $\boldsymbol{H} \parallel c$ ($\theta = 0$).

Since at the temperature of the experiment (1.7 K) the fluorine spin-lattice relaxation time is long, the signal may result to be partially saturated. This circumstance does not affect the shift of the resonance signal but it may distort the amplitude of the echo.

The determination of the correct orientation of the single crystals presented an additional challenge because, particularly in Cr_8, it is difficult to identify the flat surface of the crystal which is parallel to the plane of the molecular ring. Thus we found convenient to orient the crystals by using the known dependence of the level crossing critical field from orientation,[8] i.e., from the polar angle θ between the axis of the ring c and the direction of the applied magnetic field. For example, in Cr_8 the dependence is shown in Fig. 3(a), with $H_c \sim 7.6$ T when $\boldsymbol{H} \parallel c$, as also visible in the level scheme in Fig. 3(c).

The measurement of the crossing field was carried out by recording the profile of the ^{1}H-NMR $1/T_1$, the proton nuclear spin lattice relaxation rate, as a function of the applied static field H, as reported in Fig. 3(b) for Cr_8. An analogous method, which relies on the first excited state level crossing, was used for Cr_7Cd and Cr_7Ni. The advantage of this method is that the correct orientation can be checked with the sample "*in situ*," ready to be measured. In fact, near the crossing field the nuclear spin relaxation rate is enhanced by the inelastic component of the longitudinal fluctuations of the magnetization, so a peak is observed in $T_1^{-1}(H)$ at $H \sim H_c$. A complete review of

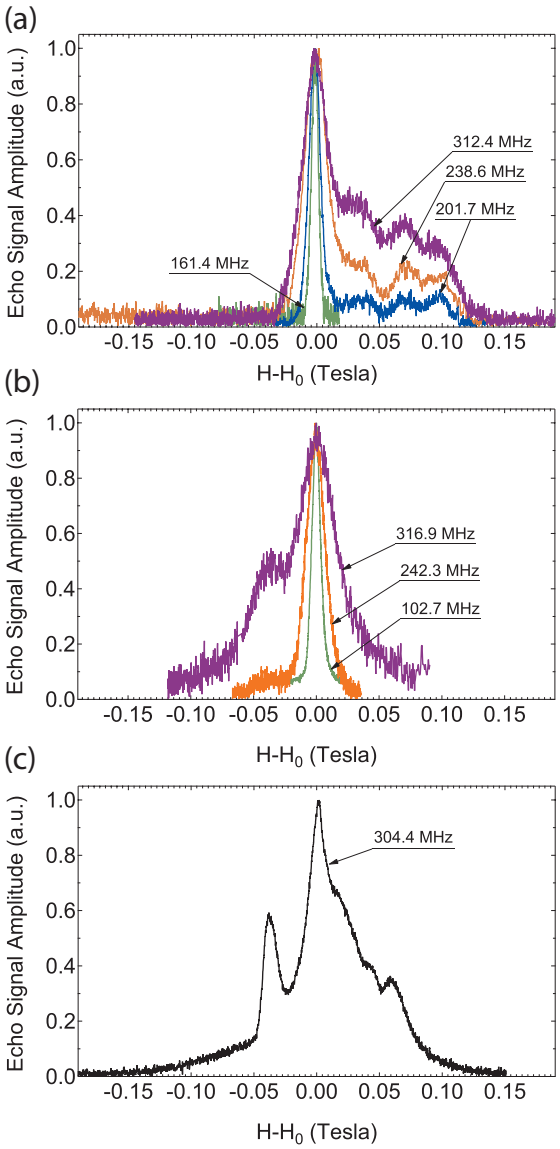

FIG. 4. Low temperature ($T = 1.7$ K)^{19}F-NMR spectra in Cr_8 single crystal at different resonance frequencies, i.e., different Larmor magnetic fields, as indicated by the tags on the graphs. The magnetic field is applied (a) parallel to the plane of the ring ($\theta = \pi/2$), (b) perpendicular to the plane of the ring ($\theta = 0^\circ$), and (c) tilted by a small angle with respect to the ring axis ($\theta \gtrsim 0$).

the dynamics at the level crossing is beyond the scope of this paper and we refer the reader to Refs. 25 and 26 for further details.

A. Cr_8

At low external magnetic fields and at $T = 1.7$ K the Cr_8 AFM ring is mostly in its $S_T = 0$ singlet ground state. The local spin expectation value at the Cr^{3+} sites should be zero, as expected for a molecular singlet state due to quantum fluctuations. This is confirmed by the ^{19}F-NMR spectra shown in Fig. 4(a) at low fields. The spectrum is a single, narrow, non-shifted line indicating the absence of hyperfine interactions between the ^{19}F nucleus and the Cr^{3+} ions. At a higher applied field the NMR line starts to broaden and four shifted lines appear at a higher resonance field (corresponding

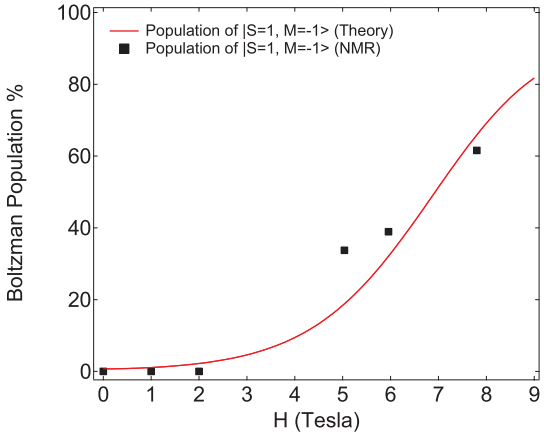

FIG. 5. Area of the three visible shifted ^{19}F-NMR lines of the Cr_8 spectra in Fig. 4(a) as a function of the resonance frequency, i.e., external field, at $T = 1.7$ K. The areas are expressed as a fraction of the total area of the spectrum. The solid line represents the calculated Boltzmann thermal population of the magnetic excited state lying above the singlet ground state, as explained in the text. The population is expressed as the fraction of $|1, -1\rangle$ state occupancy over the total population of the ground state $|0, 0\rangle$ and the first excited energy level.

to a negative local field, i.e., anti-parallel to the applied field). Only the amplitude of the shifted lines depends on the applied field while the resonance positions do not, as reported in Figs. 4(a) and 4(b).

The appearance of the shifted lines is consistent with the thermal excitation of rings from the singlet ground state to the first excited state, as the energy difference between these states decreases with increasing magnetic field, as also reflected by the increase of the local spin expectation value (see Fig. 2). The remarkable point is, however, that as the external field increases the shifted lines increase as well in intensity, but the shift value does not change. For the analysis of the experimental data it is useful to plot the integrated intensity of the three visible shifted lines as a function of the magnetic field, as reported Fig. 5. We also plot on the same graph the functions representing the Boltzmann thermal population of the excited magnetic level, as will be further discussed in Sec. V in terms of the evolution of the local spin density with the field.

The four shifted lines correspond to the four nonequivalent ^{19}F nuclei in the ring (one of the lines is not visible because its shift is small and it superimposes to the intense central line coming from the contribution of the rings in the $|S = 0, M = 0\rangle$ state). These four groups of two nuclei each are nonequivalent due to the anisotropic hyperfine interaction.

More measurements were performed in the Cr_8 single crystal with the external magnetic field oriented perpendicular to the plane of the ring ($\theta = 0$). The results are shown in Fig. 4(b); as can be seen, only one negatively shifted line is observed as the field increases contrary to the spectra obtained for $\theta = \pi/2$. As the angle is tilted slightly away from the ($\theta = 0$) condition, the lines with positive shift observed in the spectra in Fig. 4(a) for $\theta = \pi/2$ start appearing, as shown in Fig. 4(c). These results indicate that the anisotropic hyperfine interaction is dominant over the isotropic component.

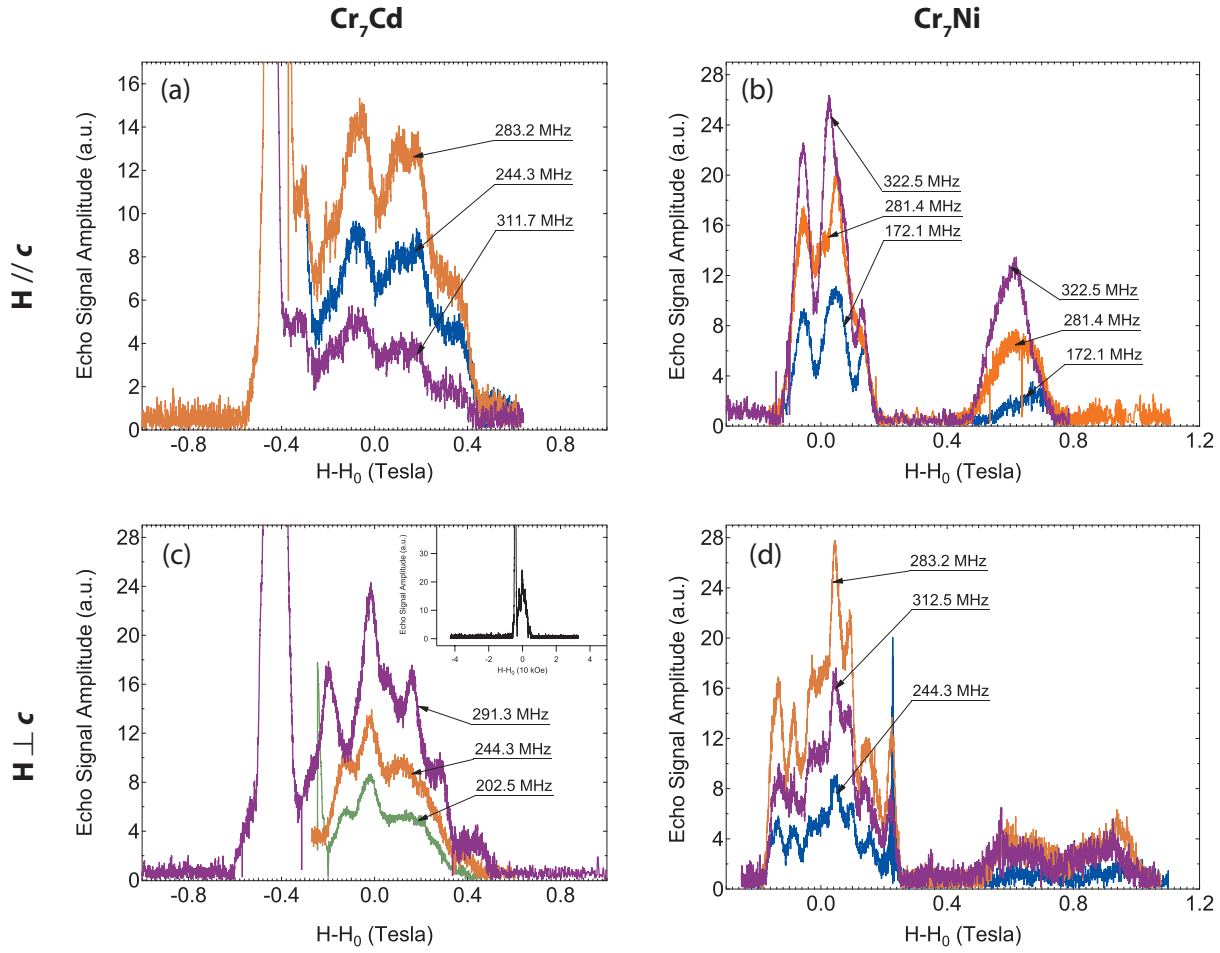

FIG. 6. ^{19}F-NMR spectra of a Cr_7Cd (plots a and c) and a Cr_7Ni single crystal (plots b and d) at $T = 1.7$ K with the applied magnetic field parallel to the plane of the ring ($\theta = 0$, plots a and b) and perpendicular to the plane of the ring ($\theta = \pi/2$, plots c and d). The value of the irradiation frequency is indicated by tags on the graphs. In the inset of (c), a spectrum collected for $\theta = \pi/2$ on a broad field range ($\Delta H = \pm 4$ T).

B. Cr_7Cd

The ^{19}F-NMR spectrum in single crystal Cr_7Cd displays a broad structure different for the two orientations of the magnetic field, as shown in Figs. 6(a) and 6(c). We could establish that no shifted signal is present on either side of the Larmor field outside a range of $H - H_0 = \pm 0.4$ T (see inset of Fig. 6(c)). Also there is no clear evidence in the spectra of a line shifted by the same amount for the two orientations of the magnetic field. Note that on the negative shift side the acquisition of the ^{19}F-NMR spectrum is made difficult by the presence of the strong unwanted signal due to the ^{1}H-NMR of the most abundant hydrogen atoms in the molecular magnet.

The absence of an orientation independent shifted signal indicates that the isotropic hyperfine interaction between the ^{19}F nucleus and the Cr^{3+} ion is smaller than the anisotropic interaction, as will be argued in Sec. V.

C. Cr_7Ni

The ^{19}F-NMR spectra in a single crystal of Cr_7Ni display for both magnetic field orientations a structured central part contained in a range of shifts $H - H_0 = \pm 0.2$ T, and a second shifted part of the spectrum at large positive shifts, as shown in Figs. 6(b) and 6(d). The signals shifted at large, positive field must arise from the F_1 and F_8 nuclei. For these ^{19}F nuclei both the dipolar and the transferred hyperfine fields produced by the neighboring Ni^{2+} and Cr^{3+} ions can be quite different and thus they do not cancel out, leading to a large resonance shift. The structured part of the spectrum around the Larmor field H_0 should be instead ascribed to the NMR signal of the F_2 to F_7 nuclei. The fact that the total spread of the spectrum in Cr_7Ni (i.e., ± 0.2 T from Fig. 6(b)) is only half the total spread in Cr_7Cd (i.e., ± 0.4 T from Fig. 6(d)) is consistent with the different local spin distribution in the two rings (from Table I).

IV. HYPERFINE INTERACTIONS

As shown in the ^{19}F-NMR spectra presented in Sec. III, the ^{19}F-NMR displays large shifts with respect to the Larmor condition; the observed shifts depend on the temperature, magnetic field, and orientation of the external magnetic field with respect to the plane of the ring. The presence of such shifts is due to the existence of large local fields at the ^{19}F nuclear positions, because the Cr^{3+}-F^- and Ni^{2+}-F^- bonds are not purely ionic. An even small degree of covalency in the bond to the paramagnetic ion requires an electron transfer

from F^- to Cr^{3+} (or Ni^{2+}). The fraction of unpaired electron remaining on the F^- ion produces a hyperfine field at the ^{19}F nucleus, which is called the "transferred hyperfine field." For a general review of the hyperfine interactions in magnetic materials we refer the reader to the seminal paper by Freeman and Watson.[27]

By referring to the principal axes system of the hyperfine constant tensor it is possible to express the component of the transferred hyperfine constant in the direction of the applied magnetic field in the form:[27–29]

$$A = A_t + A_\sigma(3\cos^2\theta_\sigma - 1) + A_\pi(3\cos^2\theta_\pi - 1). \quad (2)$$

A_t accounts for the isotropic contribution due to the s-electron polarization. The anisotropic terms $A_\sigma(3\cos^2\theta_\sigma - 1)$ and $A_\pi(3\cos^2\theta_\pi - 1)$ describe the contributions due to the polarization of the 2p orbitals of the F^- ion.

A_σ is the transferred hyperfine constant associated to the p_σ F^--Cr^{3+} bonds whose electron density is localized along the F^--Cr^{3+} internuclear axis. θ_σ is the angle between the direction of the p_σ bond and the magnetic field. Analogous definitions hold for A_π and θ_π where p_π bonds are characterized by electron density perpendicular to the F^--Cr^{3+} internuclear axis.

We will adopt the simplifying assumption that these orbitals are the p_σ bonds with the lobe of the 2p orbital along the line joining the Cr^{3+} ion with the F^- ion and the two p_π bonds respectively with the lobes perpendicular to the line connecting the two ions. A_σ is the transferred hyperfine constant associated to the p_σ bonds while θ_σ is the angle between the direction of the p_σ bond and the magnetic field. Analogous definitions hold for A_π and θ_π.

It is useful to recall that the expression of the direct isotropic hyperfine constant A_s for a single, unpaired s electron in a free atom is

$$A_s = \frac{8\pi\mu_0}{3} g\gamma_B\gamma_N\hbar|\Psi(0)|s^2 \quad (3)$$

yielding for the atomic 2s wave function in the isolated F atom[30] $A_{2s} = 1.57\ \mathrm{cm}^{-1}$, that translates into an internal field at the ^{19}F nucleus:

$$H_{2s}(F) = \frac{2\pi c}{\gamma_N} A_{2s}(\mathrm{cm}^{-1}) = 588\ \mathrm{T}/\mu_B. \quad (4)$$

The conversion between cm^{-1} and Tesla is $A(\mathrm{Tesla}) = \frac{2\pi c}{\gamma_N} A(\mathrm{cm}^{-1}) = 0.75 \times 10^3 A(\mathrm{cm}^{-1})$. The isotropic transferred hyperfine constant A_t in Eq. (2) is due to the hybridization of the 2s fluorine orbital with the d orbital of the magnetic ion. The large value of the atomic hyperfine constant in Eq. (4) shows that even a small fraction of unpaired 2s electron in the F^--Cr^{3+} bond can generate a large transferred hyperfine field at the ^{19}F nucleus.

In a similar way the expression for the hyperfine field generated by a single, unpaired 2p electron in the isolated F atom is

$$A_{2p} = \frac{2}{5}\pi g\gamma_B\gamma_N\hbar\left\langle\frac{1}{r^3}\right\rangle_{2p}. \quad (5)$$

The expression is obtained by averaging the nucleus-electron dipolar interaction over the 2p wave function. The angular dependence of the dipolar interaction is averaged over the $2p_x$, $2p_y$, and $2p_z$ components of the 2p wave function and thus yields a numerical factor independent of the orientation. Under this hypothesis, the theoretical calculation based on atomic wave functions yields[31] $A_{2p}(F) = 0.044\ \mathrm{cm}^{-1}$, which translates into an internal field at the nucleus

$$H_{2s}(F) = \frac{2\pi c}{\gamma_N} A_{2p}(\mathrm{cm}^{-1}) = 16.5\ \mathrm{T}/\mu_B. \quad (6)$$

It should be noted that even for a purely ionic bond an internal field at the kth ^{19}F nuclear site can arise from the classical dipolar interaction between the ^{19}F nuclear magnetic moment and the electronic magnetic moments of nearby Cr^{3+} (Ni^{2+}) ions. This contribution can be calculated easily in the point-dipole approximation from the knowledge of the crystal structure and the lattice parameters:

$$H_{\mathrm{dip},k} = \sum_{\substack{i=1\cdots8\\ j=1\cdots N}} \frac{\mu_0}{4\pi}\left(\frac{3\boldsymbol{r}_{ijk}\cdot(\boldsymbol{\mu}_{ij}\cdot\boldsymbol{r}_{ijk})}{r_{ijk}^5} - \frac{\boldsymbol{\mu}_{ij}}{r_{ijk}^3}\right), \quad (7)$$

where the i index runs over the 8 magnetic sites and the j index runs over the N molecular sites of the crystal. $\boldsymbol{r}_{ijk}$ is the distance between the kth F site of one molecule and the ith local magnetic moment of the jth molecule of the crystal, $\boldsymbol{\mu}_{ij}$.

We calculated the classical dipolar contribution for all ^{19}F sites in the different rings, restricting the lattice sum in Eq. (7) to intramolecular interactions only (i.e., we dropped the j index), since the intermolecular terms are negligible; the estimated relative uncertainty due to having neglected the long-ranged intermolecular interactions is below 0.05%. On the other hand, a sizable error is introduced by extending the point charge approximation to the nearest neighbors Cr ions. A detailed investigation of the differences between the exact result and the point charge approximation for d-electrons at variable distances is given in Ref. 32.

On the basis of the results for distances of the order of $0.2 \div 0.3$ nm (relevant here) we estimate an uncertainty in our calculated dipolar hyperfine fields of the order of 20%. A more precise estimate of the dipolar field appears to be unnecessary here since the dipolar field adds anyway to the transferred hyperfine field, which is derived from fitting the NMR spectra, and is thus affected by a substantial uncertainty (see Table II) .

The results of our calculations indicate that the eight ^{19}F sites are nonequivalent and that the internal dipolar field H_{dip} varies, assuming a wide range of positive and negative values with maximum absolute value $H_{\mathrm{dip,max}} = \mathrm{Max}(|H_{\mathrm{dip}}|) \lesssim 0.1\,\mathrm{T}$ for Cr_8, $H_{\mathrm{dip,max}} \lesssim 0.5\,\mathrm{T}$ for Cr_7Cd and $H_{\mathrm{dip,max}} \lesssim 0.4\,\mathrm{T}$ for Cr_7Ni. This classical dipolar internal field can therefore contribute to the ^{19}F-NMR measured shifts. Furthermore, the distribution of dipolar fields due to nonequivalent sites can explain the large width of each individual NMR line. In the following analysis we will take into account both the classical dipolar fields calculated within the point-dipole approximation and the unknown isotropic and anisotropic

TABLE II. Calculated expectation values (in Tesla units) of the hyperfine local fields at the fluorine nucleus along the direction of the external field for Cr_8, Cr_7Cd, and Cr_7Ni: H_{dip} is the classical dipolar field calculated in the point charge approximation, H_i and H_a are, respectively, the transferred isotropic and anisotropic hyperfine fields obtained from the fits of the NMR spectra. H_{tot} is the sum of the three contributions. Only fluorine sites 1, 3, and 5 are reported, as a representative set. The relative error on H_{dip} is 20%. No error is reported for H_i and H_a since an estimate of the error on the two terms separately cannot be given. To estimate the error on H_{tot} we assumed an uncertainty on $H_i + H_a$ equal to half of the width of the spectral component associated to a given fluorine site.

	Site	H_{dip}	H_i	H_a	H_{tot}
		Cr_8			
$\theta = 0$	F_1	-0.060 ± 0.012	-0.023	0.106	0.023 ± 0.025
	F_3	-0.056 ± 0.011	-0.023	0.099	0.019 ± 0.024
	F_5	-0.054 ± 0.011	-0.023	0.105	0.028 ± 0.024
$\theta = \pi/2$	F_1	0.051 ± 0.010	-0.023	-0.094	-0.065 ± 0.017
	F_3	0.012 ± 0.002	-0.023	-0.017	-0.028 ± 0.009
	F_5	0.047 ± 0.009	-0.023	-0.089	-0.065 ± 0.016
		Cr_7Cd			
$\theta = 0$	F_1	-0.272 ± 0.054	-0.097	0.530	0.160 ± 0.082
	F_3	-0.022 ± 0.004	-0.010	0.016	-0.016 ± 0.032
	F_5	-0.050 ± 0.010	-0.008	0.084	0.027 ± 0.038
$\theta = \pi/2$	F_1	0.046 ± 0.009	-0.093	-0.071	-0.118 ± 0.037
	F_3	-0.111 ± 0.022	-0.011	0.195	0.073 ± 0.050
	F_5	0.222 ± 0.044	-0.010	-0.400	-0.188 ± 0.072
		Cr_7Ni			
$\theta = 0$	F_1	-0.067 ± 0.013	-0.920	0.356	-0.630 ± 0.058
	F_3	-0.086 ± 0.017	-0.009	0.164	0.069 ± 0.062
	F_5	-0.079 ± 0.016	-0.009	0.154	0.066 ± 0.061
$\theta = \pi/2$	F_1	0.220 ± 0.044	-0.602	-0.230	-0.611 ± 0.089
	F_3	-0.185 ± 0.037	-0.012	0.346	0.149 ± 0.082
	F_5	0.209 ± 0.042	-0.013	-0.389	-0.193 ± 0.087

transferred hyperfine fields, which will be treated as adjustable fit parameters.

V. ANALYSIS OF THE ^{19}F-NMR SPECTRA

In this section we derive the value of the ^{19}F-Cr^{3+} and F^--Ni^{2+} isotropic and anisotropic transferred hyperfine constants by fitting the ^{19}F spectra in the different magnetic rings presented in Sec. III.

In order to provide an idea of the relative weight of the contributions from the classical dipolar field and the transferred hyperfine fields for some representative fluorine sites we refer the reader to Table II. Note that the labels "transferred isotropic hyperfine field" (H_i) and "transferred anisotropic hyperfine field" (H_a) in the caption of Table II might be misleading and have been so chosen for lack of a better option: the terms "isotropic" and "anisotropic" describe the nature of the hyperfine interaction that produces the local field contribution, they are not intended to reflect the degree of isotropy of the local fields themselves. This is the reason why in Table II the H_i values for Cr_7Ni differ for $\theta = 0$ and $\theta = \pi/2$: the underlying hyperfine interaction is indeed isotropic, but the strong anisotropy of the local magnetic moments (see Sec. IV and Table I) ultimately leads to an anisotropic H_i hyperfine field.

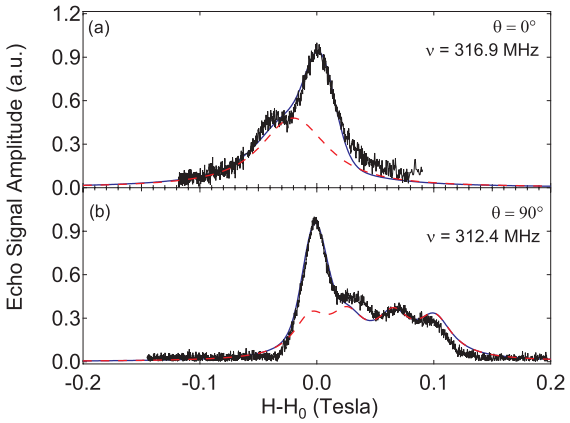

FIG. 7. Experimental and simulated ^{19}F-NMR spectra of the Cr_8 single crystal, with (a) $\boldsymbol{H} \parallel c$ and (b) $\boldsymbol{H} \perp c$. The solid line contains the contributions from both the $S_T = 0$ and $S_T = 1$ rings; the dashed red line represents the contributions from the $S_T = 1$ magnetic rings only.

A. Cr_8

The structure of the spectra observed at high magnetic field in Cr_8 (Figs. 4 and 7) arises from the combination of a narrow line centered at the Larmor field H_0, originating from ^{19}F nuclei of the rings in the $S_T = 0$ ground state (no shift, since the local average spin $\langle s \rangle = 0$), and shifted lines arising from rings in the excited magnetic triplet state ($S_T = 1$) where the local average spin value is the same on every Cr^{3+} ion and given by $\langle s \rangle = S_T/8 = 0.125$. It should be pointed out that the structure in the Cr_8 spectra arising from the rings in the excited magnetic triplet state $|S_T = 1, M = -1\rangle$ can only be observed if the average lifetime τ_{LT} of the Cr_8 ring on the excited state is longer than $1/\Delta\omega$, where $\Delta\omega$ is the total spread of the Cr_8 spectrum, i.e., the NMR shutter speed. The NMR shutter speed can be expressed also as the inverse of the free induction decay time, τ_{FID}. We can conclude that in the investigated system the lifetime, τ_{LD}, of the excited state at $T \sim 1.7$ K must be longer than 10 μs, since $\tau_{FID} \sim 5$–10 μs.

This interpretation is corroborated by the plot in Fig. 5. In fact, the separation between the ground state and the lower branch of the triplet excited state is 10 K at zero field and it reduces linearly as the field increases, as result of the Zeeman splitting of the magnetic excited state, thus increasing the thermal population of rings in the excited state. Since the area of each shifted NMR line is proportional to the number of ^{19}F nuclei contributing to the given line, the area is found to depend on the external magnetic field following the statistical population of the excited state as shown in Fig. 5 by the full line given by $P_{E'} = (1/Z)Exp(-\beta E'(H))$, where $E'(H)$ is the field-dependent eigenvalue of the first excited state. Thus we can conclude that scenario b), discussed in Sec. II B, is the one that applies to the present case.

The deviation of the experimental points from the curve describing the population of the excited magnetic state in Fig. 5 is most likely due to effects of the saturation of the NMR lines, resulting from the ^{19}F spin-lattice relaxation time being field-dependent and of the order of the NMR repetition rate, as explained in Sec. III.

Let's examine the case $\boldsymbol{H} \parallel c$ in detail: since all local magnetic moments are directed along the static applied field,

the classical dipolar field generated by the moments at the F sites is mostly anti-parallel to the field; this is simply due to each F^- ions being positioned mid-way between a couple of Cr^{3+} ions. Thus, the first-neighbor dipolar field on each ^{19}F nucleus amounts to $H_{dip} \sim -0.06$ T, which should be added to the transferred hyperfine internal field to give the measured shifts. Adding both dipolar and transferred hyperfine fields (Eq. (2)) one has for the shift of the NMR lines corresponding to a given eigenstate $|\alpha\rangle$ of $\mathcal{H}$ (Eq. (1):

$$\begin{aligned} H - H_0 &= -H_{dip} + (A_i g\langle s\rangle_i + A_{i+1} g\langle s\rangle_{i+1}) \\ &= -H_{dip} + 2\{A_{t,F-Cr} + A_\sigma(3\cos^2\theta_\sigma - 1) \\ &\quad + A_\pi[(3\cos^2\theta_{\pi'} - 1) + (3\cos^2\theta_{\pi''} - 1)]\} g\langle s\rangle, \end{aligned} \tag{8}$$

where $\langle s\rangle = \langle\alpha|s|\alpha\rangle$ and the hyperfine constant of the local spin in the ground state $|0, 0\rangle$ and in the first excited state $|1, -1\rangle$ is assumed to be the same for the Cr^{3+} on either side of a given Fluorine. The shift observed for the only NMR line in Fig. 4(b) is about -0.04 T and should be given by Eq. (8) with $\theta_\sigma = \pi/2$ and $\theta_{\pi'} = 0$, $\theta_{\pi''} = \pi/2$, keeping into account that $H_{dip} \sim -0.06$ T. We assume here that the lobe of the 2p orbital contributing to the σ bond is along the ^{19}F-^{53}Cr internuclear line, while the two 2p orbitals contributing to the π bond are along the perpendicular to the ring plane and the perpendicular to the σ bond in the ring plane, respectively. Thus one can derive from Eq. (8) the value $A_{t,F-Cr} - (A_\sigma - A_\pi)_{F-Cr} \simeq 0.2\,\mathrm{T}/\mu_B$, when we assume in Eq. (8) $g\langle s\rangle = 0.25\ \mu_B$ (since in the excited state each Cr^{3+} carries a $\langle s\rangle = 1/8$ spin unit). In Fig. 7 we show the result of a simulation of one of the spectra from Fig. 4(a) and a corresponding one from Fig. 4(b) for the two different orientations of the crystal.

In order to determine separately the isotropic, A_t, and anisotropic, $A_\pi - A_\sigma$, terms in the transferred hyperfine interaction we have fitted the NMR spectra to a sum of Lorentzian shaped components, having the same width and areas proportional to the number of ^{19}F nuclei contributing to the given line. The presence of four shifted lines is perfectly consistent with the presence of four groups of two ^{19}F nuclei in the ring, each with different angles θ_σ and θ_π (in the case $\boldsymbol{H} \perp c$) and thus four different shifts. The simulated spectra reported in Fig. 7 yield a satisfactory agreement by choosing $A_{t,F-Cr} = -0.046\,\mathrm{T}/\mu_B$ and $A_\sigma - A_\pi = -0.25\,\mathrm{T}/\mu_B$. The small negative isotropic contribution has been chosen to adjust the position of the calculated ^{19}F-NMR lines for the $\boldsymbol{H} \perp c$ geometry. The occurrence of a very small isotropic hyperfine constant is consistent with the fact that no orientation independent shifted line is observed in the Cr_8 spectra as well as the Cr_7Cd spectra discussed below. It should be stressed that the fits refer only to the spectrum originating from the rings in the excited magnetic state while the non-shifted NMR line at the Larmor field originates from the rings in the singlet ground state (see Fig. 7).

B. Cr_7Cd

The interpretation of the ^{19}F-NMR spectra of the Cr_7Cd molecule presents a much greater challenge with respect to Cr_8, since we experimentally observed a very structured spectrum for both investigated geometries. If we take into account only the transferred hyperfine interactions, we expect a structure around zero shift in the ^{19}F-NMR spectrum of Fig. 6 due to the ^{19}F nuclear sites that are located away from the Cd^{2+} ion, namely F_{2-7}, according to the labeling scheme of Fig. 1. The vector sum of the hyperfine fields produced by these moments at the ^{19}F nucleus totals to a small local hyperfine field value. On the other hand, nuclei at sites F_1 and F_8 experience the hyperfine field produced by only one Cr^{3+} magnetic moment, namely Cr_1 and Cr_7, respectively (see Fig. 1). As a consequence, the ^{19}F-NMR line from the F_1 and F_8 nuclei should be observed at a much greater shift with respect to the F_{2-7} sites.

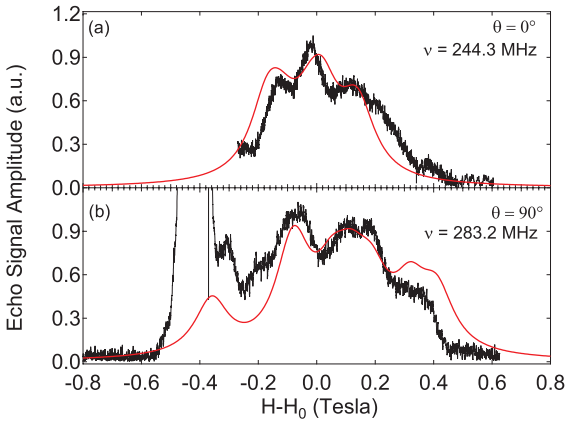

FIG. 8. Experimental and simulated ^{19}F-NMR spectra of the Cr7Cd single crystal, with (a) $\boldsymbol{H} \parallel c$ and (b) $\boldsymbol{H} \perp c$.

By assuming that the Cr^{3+}-^{19}F transferred hyperfine interaction constants in Cr_7Cd has the same value as what was found in Cr_8, i.e., $A_t \simeq -0.046\,\mathrm{T}/\mu_B$ and $A_\sigma - A_\pi = -0.25\,\mathrm{T}/\mu_B$, one expects for the case $\boldsymbol{H} \perp c$ two shifted lines for the F_1 and F_8 fluorine sites, located at $H - H_0 = (A_t + A_\sigma(3\cos^2\theta_\sigma - 1) + A_\pi(3\cos^2\theta_{\pi'} - 1) + A_\pi(3\cos^2\theta_{\pi''} - 1))g\langle s\rangle = (A_t - (A_\sigma - A_\pi))g\langle s\rangle = -0.41$ T, where we used $g\langle s\rangle = -2.1\ \mu_B$ for the Cr_1 and Cr_7 sites (see Fig. 2) and the expectation values refer to the ground state of the electron-spin Hamiltonian.

However, the calculated local dipolar field for F_1 and F_8 is also about ~ -0.2 T, so the two interactions balance each other out, shifting these two lines closer to zero. The remaining sites, F_2 to F_7, experience a small effective dipolar field, following arguments similar to the case of the transferred hyperfine interaction. The resulting structure is then contained within the range $-0.15 < H < +0.15$ T. As can be seen by the simulated spectra for Cr_7Cd in Fig. 8, one finds a reasonable agreement by using the calculated dipolar fields and the same hyperfine constants as in Cr_8.

The shape of the simulated spectra are also in reasonable agreement with the experimental observation. Note that for the case $\boldsymbol{H} \perp c$, since the azimuthal angle ϕ is not experimentally known, the reported simulated curves corresponds to the value of ϕ that yields the closest match to the experimental data ($\phi \simeq 3\pi/4$ with respect to the axis joining the center of the ring with the Cd^{2+} ion).

C. Cr_7Ni

Cr_7Ni ^{19}F-NMR spectra in Fig. 6 show, besides a structure around the Larmor field similar to the one for Cr_7Cd, one or more lines with a large positive shift.

In the $\boldsymbol{H} \parallel c$ configuration, the electronic classical dipolar field yields a somewhat less scattered distribution of resonance lines around the zero shift position with respect to the Cr_7Cd spectra; the highest calculated dipolar field is $H_{\mathrm{dip,max}} \sim -0.08$ T (to be compared to $H_{\mathrm{dip,max}} \sim -0.25$ T in Cr_7Cd). This is consistent with the presence of the substitutional Ni^{2+} ion with $g\langle S\rangle \sim 0.8$, that counters the dipolar fields produced at the F_1 and F_8 sites by the two flanking Cr^{3+} ions (Cr_1 and Cr_8), having $g\langle s\rangle \sim -1.3\ \mu_B$.

We now take into account the transferred hyperfine Cr–F and Ni–F interactions. With an argument similar to the one used above in the case of Cr_7Cd, we reasonably assume that the most shifted signals, at about +0.6 T for $\boldsymbol{H} \parallel c$ (Fig. 6(b)) and in the range $0.5 < H < 1$ T for $\boldsymbol{H} \perp c$ (Fig. 6(d)), originate from ^{19}F nuclei at site F_1 and F_8. As shown in Table I, the local moment of Ni^{2+} is opposite to the one of Cr_1 and Cr_7 and has a lower absolute value. Thus, the hyperfine interaction at the F_1 and F_8 nuclear sites does not cancel out completely, yielding a sizable NMR shift if compared to the shifts experienced by sites F_{2-7}. Additionally, the experimental results seem to suggest that the isotropic and anisotropic component of $A_{\mathrm{F\text{-}Cr}}$ are much different in sign and magnitude with respect to the respective components of $A_{\mathrm{F–Ni}}$, resulting in a dramatic contribution to the total shift.

On the other hand, the ^{19}F nuclei at sites F_{2-7} experience the field produced by opposite and almost equal Cr^{3+} local moments on either site of the bridging bond, giving rise to slightly shifted NMR signals.

We will now extract information about the F–Ni hyperfine interaction from the most shifted lines in Figs. 6(b) and 6(d). For these lines one expects a total shift given by (see Eq. (8))

$$H - H_0 = -H_{\mathrm{dip}} + [A_{\mathrm{F-Cr}} g\langle s\rangle_{\mathrm{Cr_{1,7}}} + A_{\mathrm{F-Ni}} g\langle s\rangle_{\mathrm{Ni}}], \quad (9)$$

where we assume $H_{\mathrm{dip}} = H_{\mathrm{dip,max}} \sim -0.08$ T.

We first consider the orientation of the field perpendicular to the plane of the ring (Fig. 6(b)). Then, by making the same assumptions about the orientations of the σ and π bonds as above and assuming the isotropic hyperfine constant for the F-Cr bond to be $A_{\mathrm{t,F-Cr}} = -0.046\ \mathrm{T}/\mu_B$, like in Cr_8 and Cr_7Cd (see Eqs. (8) and (9)), one has

$$H - H_0 = -H_{\mathrm{dip}} + [A_{\mathrm{t,F-Cr}} - (A_\sigma - A_\pi)_{\mathrm{F-Cr}}] g\langle s\rangle_{\mathrm{Cr_{1,7}}} + [A_{\mathrm{t,F-Cr}} - (A_\sigma - A_\pi)_{\mathrm{F-Ni}}] g\langle s\rangle_{\mathrm{Ni}}. \quad (10)$$

From Table I and by considering the case $\boldsymbol{H} \parallel c$ we can deduce the following values for the local spin densities: $g\langle s\rangle_{\mathrm{Cr_{1,7}}} = -1.3\ \mu_B$ and $g\langle s\rangle_{\mathrm{Ni}} = 0.8\ \mu_B$. Then by using the experimental value of the shift, i.e., $H - H_0 = +0.6$ T (see Fig. 6(d)) and substituting the known values for the $A_{\mathrm{t,F-Cr}}$ and $(A_\sigma - A_\pi)_{\mathrm{F-Cr}}$ constants found for Cr_8 and Cr_7Cd one derives:

$$A_{\mathrm{t,F-Ni}} - (A_\sigma - A_\pi)_{\mathrm{F-Ni}} = 0.98\ \mathrm{T}. \quad (11)$$

In order to determine separately the isotropic and anisotropic part of the transferred hyperfine constant for the F–Ni bond one should measure spectra at different orientations of the magnetic field. In the present case it was only possible to measure the spectrum for $\boldsymbol{H} \parallel c$ and $\boldsymbol{H} \perp c$, as shown in Fig. 6. Still, it is possible to achieve better estimate of the hyperfine constants by resorting once again to the numerical simulation of the ^{19}F-NMR spectra. It should be noticed that the fact that for $\boldsymbol{H} \perp c$ the shift is still positive and large but with more than one line seems to indicate that the absolute value of the isotropic contribution to the transferred hyperfine constant, $A_{\mathrm{t,F–Ni}}$, is much higher than the anisotropic contribution, $(A_\sigma - A_\pi)_{\mathrm{F–Ni}}$.

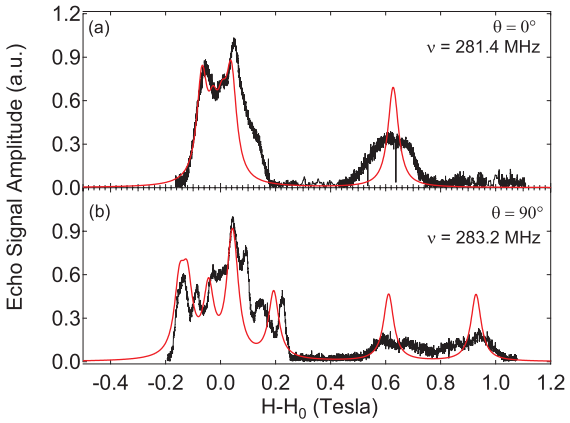

FIG. 9. Experimental and simulated ^{19}F-NMR spectra of the Cr_7Ni single crystal, with (a) $\boldsymbol{H} \parallel c$ and (b) $\boldsymbol{H} \perp c$.

The simulated spectra reported in Figs. 9(a) and 9(b) have been calculated by slightly readjusting the value of the anisotropic contribution $(A_\sigma - A_\pi)_{\mathrm{F-Cr}}$ to the Cr-F hyperfine constant to $-0.18\ \mathrm{T}/\mu_B$, and $A_{\mathrm{t,F-Cr}} = -0.04\ \mathrm{T}/\mu_B$. These values satisfactorily describe the central part of the spectrum in both orientations, $\boldsymbol{H} \parallel c$ and $\boldsymbol{H} \perp c$. Accordingly, the values for $A_{\mathrm{t,F-Ni}}$ and $(A_\sigma - A_\pi)_{\mathrm{F-Ni}}$ have been set to $1.15\ \mathrm{T}/\mu_B$ and $0.18\ \mathrm{T}/\mu_B$, respectively. Remarkably, the calculated values for the F–Ni transferred hyperfine fully satisfy Eq. (11), since $A_{\mathrm{F-Ni}} = A_{\mathrm{t,F-Ni}} - (A_\sigma - A_\pi)_{\mathrm{F-Ni}} = 0.97\ \mathrm{T}/\mu_B$, also considering that it is reasonable to assume a relative error of roughly 10%–15% on both contributions to $A_{\mathrm{F–Ni}}$.

VI. DISCUSSION

The values of the transferred hyperfine constants found here in the AFM rings can be compared with values reported in the literature in insulating paramagnets. The discussion that follows is based on the results summarized in Table III. All values found in the literature were converted from cm^{-1} to Tesla/μ_B by using $A(\mathrm{Tesla}) = A(\mathrm{cm}^{-1}) \cdot 0.75 \times 10^3$ and by dividing either by the g factor or by the number of Bohr magnetons of the magnetic ion depending on the notation adopted by the authors.

The F^--Cr^{3+} transferred hyperfine constant was investigated in K_2NaCrF_6 crystal.[33] A very small negative value was reported for the isotropic term $A_t(\mathrm{iso}) = -0.04 \pm 0.02\ \mathrm{T}/\mu_B$ while the difference of the anisotropic terms (Eq. (2)) is $A_\sigma - A_\pi = -0.27 \pm 0.04\ \mathrm{T}/\mu_B$. Since magnetic electrons in Cr^{3+} can only form π bonds with the F^- ions,[33] to first

TABLE III. Summary of the isotropic and anisotropic transferred hyperfine constants for Cr_8, Cr_7Cd, and Cr_7Ni obtained in the present investigation (expressed in Tesla/μ_B units). We also report values from the literature of the hyperfine constants for the fluorine nucleus in other paramagnetic crystals to facilitate the comparison discussed in Sec. VI.

	Cr-F hyperfine constants	
	A_t	$A_\sigma - A_\pi$
Cr_8	-0.04 ± 0.02	-0.25 ± 0.07
Cr_7Cd	-0.04 ± 0.02	-0.25 ± 0.07
Cr_7Ni	-0.06 ± 0.02	-0.25 ± 0.07
K_2NaCrF_6	-0.04 ± 0.02	-0.27 ± 0.04
	Ni-F hyperfine constants	
Cr_7Ni	1.15 ± 0.3	0.18 ± 0.05
NiF_2	1.36 ± 0.1	0.34 ± 0.03
$KNiF_3$	1.47 ± 0.2	0.41 ± 0.05

approximation $A_\sigma = 0$; thus, the negative value of $A_\sigma - A_\pi$ is consistent with a dominant contribution in the covalent bond of the 2p electron of the F^- ion with a prevalence of π bonding.

The F^--Ni^{2+} transferred hyperfine constant was investigated in $KNiF_3$[34] and in NiF_2.[35,36] The values reported are $A_t(\text{iso}) = 1.47 \pm 0.15\,\text{T}/\mu_B$ for $KNiF_3$ and $A_t(\text{iso}) = 1.36 \pm 0.1 \div 1.58 \pm 0.1\,\text{T}/\mu_B$ for NiF_2, where the two different values refer to the two nonequivalent bonds in the crystal. In both Ni crystals it was found that the anisotropic terms in the hyperfine constants are large, being about 25% of the isotropic terms arising mainly from A_σ related to the σ bonds (see Eq. (2)).

The values of the transferred hyperfine constant found in Cr_7Cd and Cr_7Ni in the present work are similar to the results obtained in the other paramagnetic crystals. For the F^--Cr^{3+} bond in Cr_8 and Cr_7Cd it was found $(A_\sigma - A_\pi)_{\text{F–Cr}} = -0.25\,\text{T}/\mu_B$ and a small negative isotropic constant $A_{\text{t,F–Cr}} = -0.04\,\text{T}/\mu_B$. This is consistent with the result in K_2NaCrF_6, i.e., a dominant A_π term in Eq. (2), where the negative sign arises from the angular dependence of the $(3\cos^2\theta_\pi - 1)$ factor. This implies a dominant 2p character of π type of the hybridization of the F^--Cr^{3+} bond with negligible 2s hybridization.

On the other hand, from the ^{19}F-NMR spectra in Cr_7Ni we infer a value $A_{\text{t,F–Ni}} = 1.15\,\text{T}/\mu_B$ for the isotropic constant and a small positive value for the anisotropic constant, $(A_\sigma - A_\pi)_{\text{F–Ni}} = 0.18\,\text{T}/\mu_B$. These values are consistent with the results in NiF_2 and $KNiF_3$. and imply a 2s hybridization and a prevalent π character of the 2p hybridization. To be more specific, an isotropic constant of $A_{\text{t,F–Ni}} = 1.15\,\text{T}/\mu_B$ would correspond to a percentage of 2s hybridization (from Eq. (4)) $f = (1.15/588) \times 100 = 0.19\%$.

VII. CONTRIBUTION TO THE ELECTRON-SPIN DECOHERENCE

In the present class of molecular nanomagnets, hyperfine interactions represent the main source of decoherence for the electron spin at low temperatures.[16] In particular, we consider the case where a linear superposition between two ground states, $|\Psi_1\rangle$ and $|\Psi_2\rangle$, of the spin Hamiltonian $\mathcal{H}$ (Eq. (1)) is generated by some external driving field. Under the effect of hyperfine interactions, the coherence between such states, $r(t) = |\langle|\Psi_1\rangle\langle\Psi_2|\rangle|$, decays due to two main contributions.[15,37] A fast contribution comes from the fact that the nuclear spins are initially in a highly mixed state. This results in a dispersion in terms of the Overhauser field, and thus of the Larmor frequency with which the relative phase between $|\Psi_1\rangle$ and $|\Psi_2\rangle$ oscillates. This decay typically takes place on a ns timescale, but its effect can in principle be canceled by applying to the electron spins refocusing pulses, such as those used here for the nuclear spins. The second contribution to the electron-spin decoherence comes from the dynamics of the nuclear spins, and specifically from its dependence on the component $|\Psi_k\rangle$ of the linear superposition. In fact, for any initial state $|\mathcal{I}\rangle$ of the nuclear spins, the decoherence factor $r(t)$ corresponds to the overlap between $|\mathcal{I}_1(t)\rangle$ and $|\mathcal{I}_2(t)\rangle$, defined as the states of the nuclear spins, conditioned upon the electron spins being in $|\Psi_1\rangle$ and $|\Psi_2\rangle$, respectively. On the timescales of interest, the dynamics of the nuclear spins, which determines the time evolution of $r(t) = |\langle\mathcal{I}_1(t)|\mathcal{I}_2(t)\rangle|$, can be traced back to independent flip-flop transitions between pairs of nuclear spins, hereafter labeled p and q: $|\uparrow_p,\downarrow_q\rangle \rightarrow |\downarrow_p,\uparrow_q\rangle$.[15,37] The electron-spin decoherence results from the number of such transitions that take place within the nuclear-spin bath, and from their dependence on the component, $|\Psi_1\rangle$ or $|\Psi_2\rangle$, of the linear superposition. It should be noted that, in order for the transition $|\uparrow_p,\downarrow_q\rangle \rightarrow |\downarrow_p,\uparrow_q\rangle$ to occur, the nuclear spins have to be equivalent. In other words, the energy difference between the initial and final states must be comparable to the amplitude of the flip-flop transition. In the presence of an applied magnetic field, nuclear spins belonging to different chemical elements are made inequivalent by their different gyromagnetic ratios. However, also nuclear spins corresponding to the same chemical element can be highly inequivalent, if they couple differently to the electron spins. These remarks apply to the role played by the F ions in the decoherence of the Cr_7M nanomagnets.

The difference between the respective magnetic moments makes the nuclear spins of the F atoms highly inequivalent with respectwo to those of the H atoms. The contribution to the electron spin decoherence of each F nucleus thus mainly comes from flip-flop transitions with other F spins. However, due to the hyperfine interactions, also the F spins are different from one another (Table III). Given the observed values of the hyperfine shifts (Table II), the energy cost of a flip-flop transition between inequivalent F spins is of the order of $1 \div 10$ neV ($0.3 \div 3$ MHz). This quantity should be contrasted with the largest amplitude of a flip-flop transition (that between neighboring F ions in the ring), which is of the order of 10^{-2} neV (3 KHz). As a result, the only possible flip-flop transitions that involve the F nuclei are those between F_1 and F_8, F_2 and F_7, F_3 and F_6, F_4 and F_5 (Fig. 1). We finally note that each of these spin pairs can undergo a flip-flop transition only if the two nuclear spins are initially anti-parallel to each other.

In conclusion, even though the F^- ions are close to the electron-spin density, their potential contribution to decoherence is strongly limited by the hyperfine interactions themselves. In fact, these make F nuclei inequivalent to one another, thus preventing the occurrence of flip-flop transitions

in most spin pairs. A further suppression of the F contribution might result from the anisotropic term of the transferred hyperfine constant, if the magnetic field is aligned along a low-symmetry direction. In fact, in this case the F nuclei would all be inequivalent.

VIII. CONCLUSIONS

A relevant result of the present investigation regards the magnetization process at low temperature in the Cr_8 homometallic ring; we deduced that, while by increasing the external magnetic field the $S_T = 0$ ground state and the lower branch of the triplet excited state $|1, -1\rangle$ approach each other, there is no sizable mixing of states with different parity all the way up to the level crossing at about 7 T. Indeed, we found a statistical distribution of rings with total spin $S_T = 0$ and local spin $\langle s\rangle = 0$ and rings with total spin $S_T = 1$ and local spin $\langle s\rangle = S_T/8$, with a lifetime of the excited state longer than a few microseconds.

The detailed knowledge of the hyperfine couplings also represents a crucial starting point for understanding the role played by the different chemical elements in the electron-spin decoherence. In fact, the relevance of such role does not depend simply on the distance between the nuclei and the magnetic ions in the nanomagnet, or on the value of the hyperfine coupling constant. It also depends on the number of energy-conserving transitions that these nuclei can actually undergo, and thus on the number of equivalent nuclei. In this respect, we note that the presence of anisotropic hyperfine interactions can reduce the number of equivalent nuclei, and thus slow down the electron-spin decoherence resulting from the dynamics of the nuclear spins.

The vast majority of the relevant nuclear spins in the Cr-based wheels is associated to the H atoms. In this case, the inequivalence of neighboring nuclei induced by their hyperfine coupling to the electron spins decreases with the distance from the magnetic ions and is, on average, less pronounced. Different approaches thus need to be applied, in order to reduce the hyperfine-induced decoherence. At the chemical level, the replacement of the H atoms with deuterium reduces the dipolar couplings between electron and nuclear spins, and thus allows a significant enhancement of the decoherence times.[16] Alternatively, quantum information can be encoded in electron-spin degrees of freedom that are (approximately) decoupled from nuclear spins, and are thus intrinsically protected from this source of decoherence, as is the case with spin chirality.[38]

ACKNOWLEDGMENTS

Ames Laboratory is operated for the US Department of Energy (DOE) by Iowa State University under Contract No. DE-AC02-07CH11358. This work at Ames Laboratory was supported by the Office of Basic Energy Science. PRIN Italian Project No. 2008PARRTS 001 by MIUR and FIRB Italian Project "Futuro in Ricerca" No. RBFR12RPD1 are thanked for partly funding the present research.

[1]M. N. Leuenberger and D. Loss, Nature **410**, 789 (2001).
[2]F. Meier, J. Levy, and D. Loss, Phys. Rev. Lett. **90**, 047901 (2003).
[3]F. Troiani, A. Ghirri, M. Affronte, S. Carretta, P. Santini, G. Amoretti, S. Piligkos, G. Timco, and R. E. P. Winpenny, Phys. Rev. Lett. **94**, 207208 (2005).
[4]P. Santini, S. Carretta, F. Troiani, and G. Amoretti, Phys. Rev. Lett. **107**, 230502 (2011).
[5]G. A. Timco, E. J. L. McInnes, and R. E. P. Winpenny, Chem. Soc. Rev. **42**, 1796 (2013).
[6]Y. Furukawa, K. Kiuchi, K.-i. Kumagai, Y. Ajiro, Y. Narumi, M. Iwaki, K. Kindo, A. Bianchi, S. Carretta, G. A. Timco *et al.*, Phys. Rev. B **78**, 092402 (2008).
[7]A. Bianchi, S. Carretta, P. Santini, G. Amoretti, Y. Furukawa, K. Kiuchi, Y. Ajiro, Y. Narumi, K. Kindo, J. Lago *et al.*, J. Magn. Magn. Mater. **322**, 1262 (2010).
[8]J. Van Slageren, R. Sessoli, D. Gatteschi, A. A. Smith, M. Helliwell, R. E. P. Winpenny, A. Cornia, A.-L. Barra, A. G. M. Jansen, E. Rentschler *et al.*, Chem. Eur. J. **8**, 277 (2002).
[9]D. M. Tomecka, V. Bellini, F. Troiani, F. Manghi, G. Kamieniarz, and M. Affronte, Phys. Rev. B **77**, 224401 (2008).
[10]G. Timco, S. Carretta, F. Troiani, F. Tuna, R. Pritchard, C. Muryn, E. McInnes, A. Ghirri, A. Candini, P. Santini, *et al.*, Nat. Nanotechnol. **4**, 173 (2009).
[11]G. A. Timco, T. B. Faust, F. Tuna, and R. E. P. Winpenny, Chem. Soc. Rev. **40**, 3067 (2011).
[12]V. Bellini, G. Lorusso, A. Candini, W. Wernsdorfer, T. B. Faust, G. A. Timco, R. E. P. Winpenny, and M. Affronte, Phys. Rev. Lett. **106**, 227205 (2011).
[13]R. Caciuffo, T. Guidi, G. Amoretti, S. Carretta, E. Liviotti, P. Santini, C. Mondelli, G. Timco, C. A. Muryn, and R. E. P. Winpenny, Phys. Rev. B **71**, 174407 (2005).
[14]F. Borsa, A. Lascialfari, and Y. Furukawa, in *Novel NMR and EPR Techniques*, edited by J. Dolinsek, M. Vilfan, and S. Zumer (Springer, Berlin, Heidelberg, 2006), pp. 297–349.
[15]F. Troiani, V. Bellini, and M. Affronte, Phys. Rev. B **77**, 054428 (2008).
[16]A. Ardavan, O. Rival, J. J. L. Morton, S. J. Blundell, A. M. Tyryshkin, G. A. Timco, and R. E. P. Winpenny, Phys. Rev. Lett. **98**, 057201 (2007).
[17]C. Schlegel, J. van Slageren, and G. Timco, Phys. Rev. B **83**, 134407 (2011).
[18]F. K. Larsen, E. J. L. McInnes, H. E. Mkami, J. Overgaard, S. Piligkos, G. Rajaraman, E. Rentschler, A. A. Smith, G. M. Smith, V. Boote *et al.*, Angew. Chem. **115**, 105 (2003).
[19]E. Micotti, Y. Furukawa, K. Kumagai, S. Carretta, A. Lascialfari, F. Borsa, G. A. Timco, and R. E. P. Winpenny, Phys. Rev. Lett. **97**, 267204 (2006).
[20]C. M. Casadei, L. Bordonali, Y. Furukawa, F. Borsa, E. Garlatti, A. Lascialfari, S. Carretta, S. Sanna, G. Timco, and R. Winpenny, J. Phys. Condens. Mater. **24**, 406002 (2012).
[21]M. L. Baker, T. Guidi, S. Carretta, J. Ollivier, H. Mutka, H. U. Güdel, G. A. Timco, E. J. L. McInnes, G. Amoretti, R. E. P. Winpenny *et al.*, Nat. Phys. **8**, 906 (2012).
[22]S. Carretta, J. van Slageren, T. Guidi, E. Liviotti, C. Mondelli, D. Rovai, A. Cornia, A. L. Dearden, F. Carsughi, M. Affronte *et al.*, Phys. Rev. B **67**, 094405 (2003).
[23]S. Carretta, P. Santini, G. Amoretti, T. Guidi, J. R. D. Copley, Y. Qiu, R. Caciuffo, G. Timco, and R. E. P. Winpenny, Phys. Rev. Lett. **98**, 167401 (2007).
[24]S. Carretta, P. Santini, G. Amoretti, M. Affronte, A. Ghirri, I. Sheikin, S. Piligkos, G. Timco, and R. E. P. Winpenny, Phys. Rev. B **72**, 060403(R) (2005).
[25]E. Micotti, A. Lascialfari, F. Borsa, M. Julien, C. Berthier, M. Horvatić, J. van Slageren, and D. Gatteschi, Phys. Rev. B **72**, 020405(R) (2005).
[26]M.-H. Julien, Z. H. Jang, A. Lascialfari, F. Borsa, M. Horvatić, A. Caneschi, and D. Gatteschi, Phys. Rev. Lett. **83**, 227 (1999).
[27]A. J. Freeman, and R. E. Watson, in *Hyperfine Interactions in Magnetic Materials*, Magnetism Vol. IIA, edited by G. T. Rado, and S. Suhl (Academic, New York, 1967).
[28]M. Tinkham, Proc. R. Soc. London, Ser. A **236**, 535 (1956).
[29]R. G. Shulman and V. Jaccarino, Phys. Rev. **108**, 1219 (1957).
[30]D. R. Hartree, Proc. R. Soc. London **151**, 96 (1935).
[31]R. G. Barnes and W. V. Smith, Phys. Rev. **93**, 95 (1954).
[32]R. Golding and L. Stubbs, J. Magn. Res. **33**, 627 (1979).
[33]R. G. Shulman and K. Knox, Phys. Rev. Lett. **4**, 603 (1960).
[34]R. G. Shulman and K. Knox, Phys. Rev. **119**, 94 (1960).
[35]R. G. Shulman, Phys. Rev. **121**, 125 (1961).
[36]J. W. Stout and R. G. Shulman, Phys. Rev. **118**, 1136 (1960).
[37]A. Szallas and F. Troiani, Phys. Rev. B **82**, 224409 (2010).

[38]F. Troiani, D. Stepanenko, and D. Loss, Phys. Rev. B **86**, 161409(R) (2012).

[39]Previous reports[6,7,19,20] have used an Hamiltonian, Eq. (1), with the negative sign in the Zeeman term, resulting in the convention, sometimes adopted in magnetism, yielding $\boldsymbol{\mu}$ parallel to $\boldsymbol{s}$.

[40]The S-mixing itself, i.e., the contribution of the $|3/2; \pm 1/2\rangle$ and $|3/2; \pm 3/2\rangle$ states to the $S_T = 1/2$ ground state eigenfunction, amounts to about 1% (squared modulus of the components of the ground state on the total-spin basis states $|S_T = 3/2\rangle$). However, the contribution of the S-mixing to the expectation values of the local spin operators on the ground state $S_T = 1/2$ may eventually end up to account for even 15%–20% of the value calculated without it. Indeed, expectation values of the local spin operators depend on the components of the ground state on the total-spin basis states ($|1/2\rangle$ and $|3/2\rangle$ due to S-mixing) and not on their squared modulus. In addition, they also depend on the matrix elements of the spin operators between these states.